AnGeo Comm., 32, 889–898, 2014
www.ann-geophys.net/32/889/2014/
doi:10.5194/angeocom-32-889-2014

Annales Geophysicae
Open Access

Effects of cold electron number density variation on whistler-mode wave growth

R. Tang[1,2,3], **D. Summers**[3], **and X. Deng**[1]

[1]Institute of Space Science and Technology, Nanchang University, Nanchang, 330031, China
[2]State Key Laboratory of Space Weather, Chinese Academy of Sciences, Beijing 100190, China
[3]Department of Mathematics and Statistics, Memorial University of Newfoundland, St. John's, Newfoundland, Canada

Correspondence to: R. Tang (tangrx@gmail.com)

Received: 8 April 2014 – Accepted: 19 June 2014 – Published: 31 July 2014

Abstract. We examine how the growth of magnetospheric whistler-mode waves depends on the cold (background) electron number density N_0. The analysis is carried out by varying the cold-plasma parameter $a =$ (electron gyrofrequency)^2/(electron plasma frequency)^2 which is proportional to $1/N_0$. For given values of the thermal anisotropy A_T and the ratio N_h/N_0, where N_h is the hot (energetic) electron number density, we find that, as N_0 decreases, the maximum values of the linear and nonlinear growth rates decrease and the threshold wave amplitude for nonlinear growth increases. Generally, as N_0 decreases, the region of $(N_h/N_0, A_T)$-parameter space in which nonlinear wave growth can occur becomes more limited; that is, as N_0 decreases, the parameter region permitting nonlinear wave growth shifts to the top right of $(N_h/N_0, A_T)$ space characterized by larger N_h/N_0 values and larger A_T values. The results have implications for choosing input parameters for full-scale particle simulations and also in the analysis of whistler-mode chorus data.

Keywords. Space plasma physics (wave–particle interactions)

1 Introduction

Whistler-mode chorus waves are intense right-hand polarized electromagnetic emissions in the magnetosphere commonly occurring in two frequency bands: a lower band 0.1–0.5$|\Omega_e|$ and an upper band 0.5–0.7$|\Omega_e|$, where $|\Omega_e|$ is the local electron gyrofrequency. Cyclotron resonant whistler-mode-wave–electron interactions are an important controlling factor in radiation belt electron dynamics. Relativistic ($\sim$ MeV) electrons can be generated in the outer radiation belt due to cyclotron resonance with chorus (Summers et al., 1998, 2002, 2007a, b; Roth et al., 1999; Meredith et al., 2003; Summers and Omura, 2007; Xiao et al., 2010; Su et al., 2014). Chorus waves can pitch-angle scatter outer zone electrons into the loss cone and induce particle loss to the atmosphere (Lorentzen et al., 2001; O'Brien et al., 2004; Thorne et al., 2005; Summers et al., 2007a, b; Ni et al., 2008; Hikishima et al., 2010). Whistler-mode waves are instrumental in limiting stably trapped electron fluxes in planetary radiation belts (Kennel and Petschek, 1966; Summers et al., 2009, 2011; Mauk and Fox, 2010; Tang and Summers, 2012).

Chorus waves typically comprise discrete "rising-tone" elements with a time-increasing frequency. The initial stage of the generation process of magnetospheric whistler-mode chorus is considered to be linear, that is, classical linear wave growth produced by an injection at the magnetic equator of an anisotropic distribution of energetic (hot) electrons. The generation of the rising-tone elements, however, requires fully nonlinear theory. Considerable progress has been made recently in developing a nonlinear cyclotron theory of the generation of whistler-mode chorus by Omura et al. (2008, 2009, 2012), with further extensions by Summers et al. (2012a, 2013). Omura et al. (2008, 2009) describe the detailed nonlinear dynamics of cyclotron-resonant electrons and postulate the formation of electromagnetic electron "holes" that result in resonant currents generating rising-tone emissions. Various aspects of this nonlinear theory have been verified by sophisticated full-scale simulations of the generation and growth of whistler-mode chorus elements by Omura et al. (2008, 2009), Hikishima et al. (2009); Hikishima et al. (2010) and Katoh and Omura (2011). Summers et al. (2012b)

analyze the nonlinear spatiotemporal evolution of whistler-mode chorus waves propagating along a magnetic field line from their equatorial source. The wave profiles exhibit convective growth, due to nonlinear wave trapping, followed by saturation, due partly to a decreasing resonant current with latitude.

The present study concentrates on the conditions required for effective nonlinear growth of whistler-mode waves at the magnetic equator, and in particular extends the work of Summers et al. (2012a, 2013). These authors treated the growth of magnetospheric whistler-mode waves in terms of a linear growth phase followed by a nonlinear growth phase. They then constructed complete time profiles of the wave amplitude by smoothly matching the solutions in the linear and nonlinear regimes. It was found that this matching procedure could only take place over a restricted "matching region" in $(N_h/N_0, A_T)$ space where A_T is the electron thermal anisotropy, N_h is the hot (energetic) electron number density, and N_0 is the cold (background) electron number density. In a complementary analysis, using a condition based on the maximum linear growth rate, Summers et al. (2013) determined a boundary in $(N_h/N_0, A_T)$ space separating a region in which only linear whistler-mode wave growth can occur from a region in which whistler-mode waves can achieve fully nonlinear growth. The whole analysis of Summers et al. (2012a, 2013) was carried out at a fixed L shell and a fixed cold electron number density N_0. That is, in terms of the cold-plasma parameter $a = |\Omega_e|^2/\omega_{pe}^2$ where $|\Omega_e|$ is the electron gyrofrequency and ω_{pe} is the electron plasma frequency, Summers et al. (2012a, 2013) assumed that a is constant (the value $a = 1/16$ was assumed to characterize the region outside the plasmasphere at or near $L = 4$). The particular objective of the present paper is to investigate how the conditions for nonlinear growth of whistler-mode waves in the magnetosphere, as determined by Summers et al. (2012a, 2013), depend on the parameter a. Thus, herein we adopt a selection of a values to represent the differing conditions in the inner magnetosphere experienced during geomagnetic disturbances including storms and substorms.

The plan of our paper is as follows. In Sect. 2, for a chosen loss cone distribution, we examine the (relativistic) linear growth rate for whistler-mode waves and its dependence on the cold-plasma parameter a and the thermal anisotropy A_T. In Sect. 3 we give a brief account of the nonlinear cyclotron resonance theory for whistler-mode waves required in the present study. This involves introducing the "total" nonlinear growth rate $\Gamma_N(t)$ and the local nonlinear growth rate $\gamma_N(t)$. As well, we describe the "chorus equations" (Eqs. 16 and 17) used to model the nonlinear growth of a chorus element, and derive the threshold wave amplitude $\tilde{B}_{th}$ required for nonlinear growth. In Sect. 4, we show how to construct the matching region in $(N_h/N_0, A_T)$ space in which smooth matching of linear and nonlinear solutions is possible, and we also construct the (generally different) parameter region

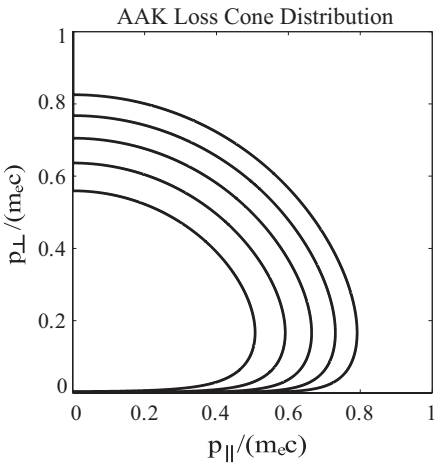

Figure 1. Contours of constant phase space density $f =$ constant, where f is given by Eq. (1), for $\beta = 0.5$, $\theta_\parallel/(m_e c) = 0.2$, $\theta_\perp/(m_e c) = 0.2$.

(with boundary 31) in which fully nonlinear wave growth can occur. Finally, in Sect. 5 we state our conclusions.

2 Relativistic linear growth rate

We assume that field-aligned electromagnetic R-mode waves are generated by a hot anisotropic electron population in the presence of a dominant cold electron population. We choose the AAK (Ashour-Abdalla and Kennel, 1978) loss cone particle distribution as the hot electron distribution function, i.e.,

$$f(p_\parallel, p_\perp) = \frac{N_h}{\pi^{3/2}\theta_\parallel\theta_\perp^2}\frac{1}{(1-\beta)}\left[\exp\left(-\frac{p_\perp^2}{\theta_\perp^2}\right) - \exp\left(-\frac{p_\perp^2}{\beta\theta_\perp^2}\right)\right]\exp\left(-\frac{p_\parallel^2}{\theta_\parallel^2}\right), \quad (1)$$

where $p_\parallel = \gamma m_e v_\parallel$ and $p_\perp = \gamma m_e v_\perp$ are the components of relativistic momentum $\boldsymbol{p} = \gamma m_e \boldsymbol{v}$, m_e is the electron rest mass, $\boldsymbol{v}$ is the electron velocity with components $v_\parallel$ and $v_\perp$, parallel and perpendicular, respectively, to the ambient magnetic field, and $\gamma = (1 - v^2/c^2)^{-1/2} = (1 + p^2/(m_e c)^2)^{1/2}$, with $v^2 = v_\parallel^2 + v_\perp^2$, $p^2 = p_\parallel^2 + p_\perp^2$, and c is the speed of light; $\theta_\parallel$ and $\theta_\perp$ are the thermal momenta of the energetic electrons parallel and perpendicular to the background magnetic field; and N_h is the hot electron number density. We require that the distribution satisfies $\int f(p_\parallel, p_\perp) d^3p = N_h$, with $d^3p = 2\pi p_\perp dp_\perp dp_\parallel$. The parameter β (where $0 < \beta < 1$) is a measure of the angular size of the loss cone. When $\beta \to 1$, distribution in Eq. (1) reduces to a particular form of the Dory–Guest–Harris loss cone distribution (Dory et al., 1965). When $\beta \to 0$, distribution in Eq. (1) reduces to a bi-Maxwellian distribution. The thermal anisotropy, defined by $A_T = T_\perp/T_\parallel - 1$, where $T_\parallel$ and $T_\perp$ are the parallel and perpendicular temperatures, is given by $A_T = (1+\beta)\theta_\perp^2/\theta_\parallel^2 - 1$ for distribution in Eq. (1).

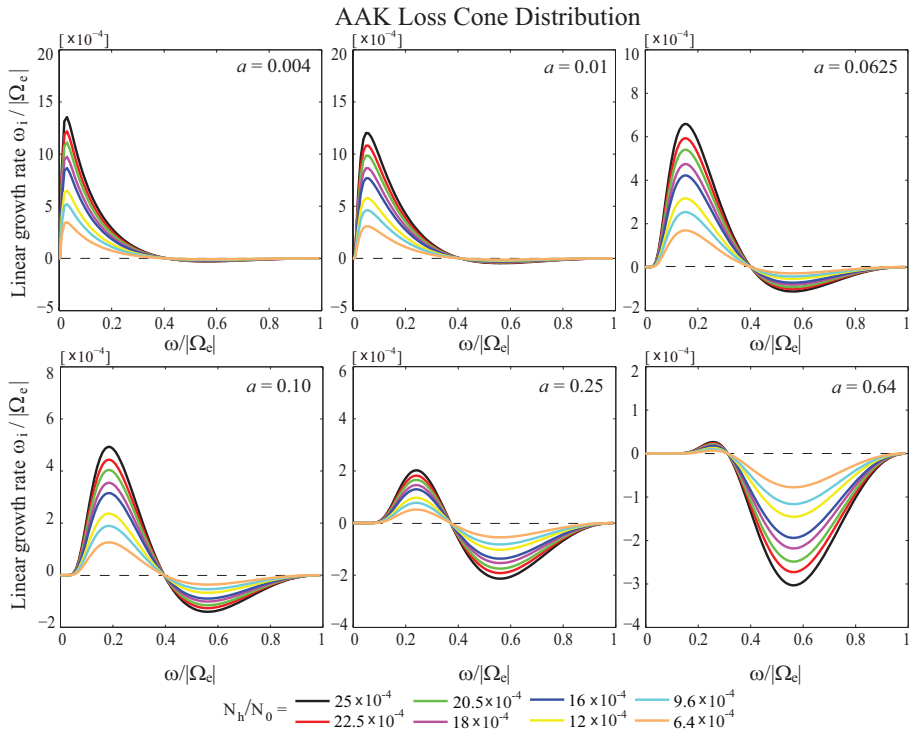

Figure 2. Relativistic linear whistler-mode wave growth rates ω_i for the AAK loss cone distribution in Eq. (1) for thermal anisotropy $A_T = 1.5$, $\theta_\parallel/(m_e c) = 0.49$, the indicated values of the electron number density ratio N_h/N_0 and the cold-plasma parameter $a = |\Omega_e|^2/\omega_{pe}^2$.

We write the cold-plasma dispersion relation for electromagnetic R-mode waves propagating parallel to an assumed uniform magnetic field in the form

$$y^2 = x^2 + \frac{x}{a(1-x)}, \tag{2}$$

where

$$x = \omega/|\Omega_e|, \quad y = ck/|\Omega_e|, \tag{3}$$

and a is the cold-plasma parameter defined by

$$a = |\Omega_e|^2/\omega_{pe}^2, \tag{4}$$

where ω is the (real) wave frequency, k is the (real) wave number, $|\Omega_e| = eB_0/(m_e c)$ is the electron gyrofrequency, $\omega_{pe} = (4\pi N_0 e^2/m_e)^{1/2}$ is the plasma frequency, $-e$ is the electron charge, N_0 is the cold electron number density, and B_0 is the magnitude of the zeroth-order magnetic field.

In Fig. 1, we show typical contours of constant phase-space density for the AAK loss cone distribution in Eq. (1) for $\beta = 0.5$, $\theta_\parallel/(m_e c) = 0.2$, $\theta_\perp/(m_e c) = 0.2$.

In Fig. 2, we plot the relativistic linear growth rates for the AAK loss cone distribution for $\theta_\parallel/(m_e c) = 0.49$, $A_T = 1.5$, the indicated values of the cold-plasma parameter a, and the various values of the electron number density ratio N_h/N_0. We find that the maximum linear growth rate increases as the number density ratio N_h/N_0 increases as expected, but it decreases as the cold-plasma parameter a increases. As a increases (or N_0 decreases), the bandwidth for wave growth ($\omega_i > 0$) slightly decreases, and the frequency at which the maximum growth rate occurs increases. Thus, the variation of a does not significantly change the frequency band for wave growth, but does affect the frequency at which the wave growth maximizes.

For the rest of the calculations and figures in this paper, we have fixed $\theta_\parallel/(m_e c) = 0.49$ as used in previous work (e.g., Summers et al., 2013).

In Fig. 3, we present the contours of constant wave frequency $\tilde{\omega}_m = \omega_m/|\Omega_e|$ at which the relativistic linear growth rate maximizes, as a function of the cold-plasma parameter a and the thermal anisotropy A_T. For smaller values of a, say $a < 0.1$, $\tilde{\omega}_m$ is only moderately dependent on the values of a and A_T.

In Fig. 4, we show two-dimensional plots of the maximum relativistic linear growth rate $\max(\tilde{\omega}_i)$ as a function of the cold-plasma parameter a and the thermal anisotropy A_T, for $N_h/N_0 = 10^{-2}$, 10^{-3}, and 10^{-4}. The white regions are regions of parameter space in which $\max(\tilde{\omega}_i)$ values are outside the typical practical range. The panels indicate that, as N_h/N_0 decreases, useful (sufficiently large) values of $\max(\tilde{\omega}_i)$ can only be obtained for larger values of A_T and smaller values of a. Figures 3 and 4 in combination are useful as an aid for selecting input parameters in future computer simulations.

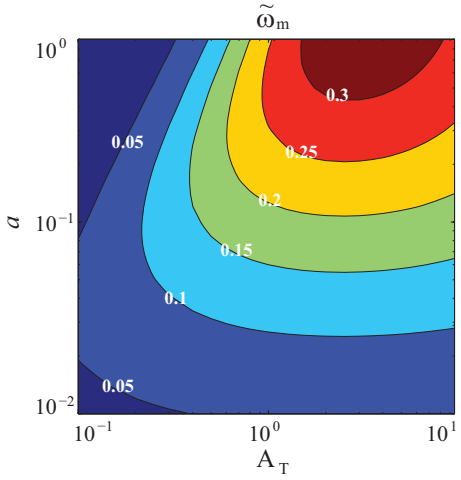

Figure 3. Contours of constant wave frequency $\tilde{\omega}_m = \omega_m/|\Omega_e|$ at which the relativistic linear growth rate maximizes, as a function of the cold-plasma parameter $a = |\Omega_e|^2/\omega_{pe}^2$ and thermal anisotropy A_T.

3 Nonlinear wave growth

Omura et al. (2008, 2009, 2012) have developed a nonlinear cyclotron resonance theory which describes the generation and growth of whistler-mode chorus waves. Summers et al. (2012a, 2013) generalized the so-called "chorus equations" (Omura et al., 2009) to an arbitrary energetic electron distribution and calculated conditions for sustained nonlinear growth. Following their work, we express the nonlinear growth rate Γ_N for field-aligned whistler-mode (R-mode) waves of frequency $\omega(t)$ and wave magnetic field amplitude $B_w(t)$ by the equation

$$\frac{dB_w}{dt} = \Gamma_N B_w, \tag{5}$$

with

$$\frac{\Gamma_N}{|\Omega_e|} = \sqrt{2} Q \chi^{3/2} \left(\frac{\xi}{\tilde{\gamma}_R}\right)^{1/2} \left(\frac{B_0}{B_w}\right)^{1/2} \left(\frac{|\Omega_e|}{\omega}\right)^{1/2} \left(\frac{V_g}{c}\right) \left(\frac{V_{\perp 0}}{c}\right)^{5/2} \frac{(m_e^2 c^2 \tilde{G})}{a N_0}, \tag{6}$$

and

$$\xi^2 = \frac{\omega(|\Omega_e| - \omega)}{\omega_{pe}^2}, \quad \chi^2 = \frac{1}{1+\xi^2}, \tag{7}$$

$$\frac{V_g}{c} = \frac{\xi}{\chi}\left[\xi^2 + \frac{\Omega_e}{2(|\Omega_e| - \omega)}\right]^{-1}, \tag{8}$$

$$\tilde{\gamma}_R = \left[1 - \left(\frac{\tilde{V}_R}{c}\right)^2 - \left(\frac{V_{\perp 0}}{c}\right)^2\right]^{-1/2}, \quad \frac{\tilde{V}_R}{c} = \chi\xi\left(1 - \frac{|\Omega_e|}{\tilde{\gamma}_R \omega}\right), \tag{9}$$

where $V_g(t)$ is the wave group speed, $\tilde{\gamma}_R(t)$ is the resonant Lorentz factor, $\tilde{V}_R(t)$ is the resonant parallel particle velocity, $V_{\perp 0}$ (= constant) is the average perpendicular particle velocity, a is the cold-plasma parameter defined by Eq. (4), and Q is the dimensionless factor that represents the depth of the electromagnetic electron hole within which nonlinear particle trapping takes place. The quantity $\tilde{G}$ is a measure of the average value of the hot electron distribution F_T trapped by the wave. We express the trapped distribution F_T as the electron ring distribution,

$$F_T(p_\parallel, p_\perp) = \Phi(p_\parallel)\delta(p_\perp - p_{\perp 0}) \tag{10}$$

with

$$p_{\perp 0} = \gamma_0 m_e V_{\perp 0}, \quad \gamma_0 = \left(1 - \frac{V_{\perp 0}^2}{c^2}\right)^{-1/2}, \tag{11}$$

where δ is the Dirac delta function, and Φ is a function of parallel particle momentum $p_\parallel$ only; $\tilde{G}$ is given by

$$\tilde{G} = \left[\int F_T dp_\perp\right]_{p_\parallel = \tilde{p}_R} = \Phi(\tilde{p}_R), \tag{12}$$

where $\tilde{p}_R = \tilde{\gamma}_R m_e \tilde{V}_R$.

Following Omura et al. (2008, 2009) and Summers et al. (2012a, 2013), we approximate the AAK distribution in Eq. (1) by the ring distribution

$$F_T(p_\parallel, p_\perp) = \frac{N_h}{\pi^2 \theta_\parallel \theta_\perp}\left(\frac{1-\beta}{1-\beta^{3/2}}\right) \exp\left(-\frac{p_\parallel^2}{\theta_\parallel^2}\right)\delta(p_\perp - p_{\perp 0}), \tag{13}$$

where

$$p_{\perp 0} = \frac{\sqrt{\pi}}{2}\left(\frac{1-\beta^{3/2}}{1-\beta}\right)\theta_\perp. \tag{14}$$

Hence from Eqs. (10)–(12) it follows that

$$\tilde{G} = \frac{N_h}{\pi^2 \theta_\parallel \theta_\perp}\left(\frac{1-\beta}{1-\beta^{3/2}}\right) \exp\left(-\frac{\tilde{p}_R^2}{\theta_\parallel^2}\right). \tag{15}$$

The normalized wave amplitude $\tilde{B}_w = B_w(t)/B_0$ and normalized frequency $\tilde{\omega} = \omega(t)/|\Omega_e|$ are found to satisfy the "chorus equations" (Omura et al., 2009; Summers et al., 2012a, 2013) given by

$$\frac{\partial \tilde{B}_w}{\partial \tilde{t}} = \frac{\Gamma_N}{|\Omega_e|}\tilde{B}_w - 5\frac{s_2}{s_0}\frac{V_g}{c}\frac{\tilde{a}}{\tilde{\omega}}, \tag{16}$$

$$\frac{\partial \tilde{\omega}}{\partial \tilde{t}} = \frac{2 s_0}{5 s_1}\tilde{\omega}\tilde{B}_w, \tag{17}$$

with $\tilde{t} = |\Omega_e| t$, and

$$s_0 = \frac{\chi}{\xi}\frac{V_{\perp 0}}{c}, \tag{18}$$

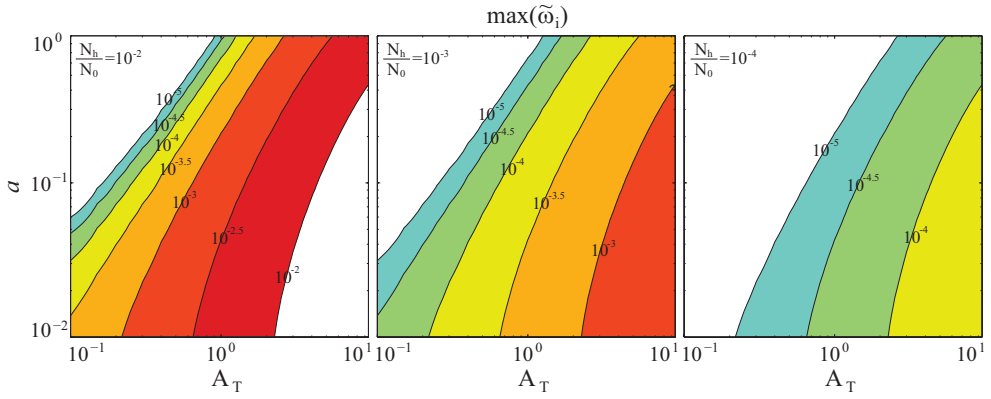

Figure 4. Two-dimensional plots of the maximum relativistic linear growth rate $\max(\tilde{\omega}_i)$ as a function of the cold-plasma parameter $a = |\Omega_e|^2/\omega_{pe}^2$ and thermal anisotropy A_T, for the indicated values of the electron number density ratio N_h/N_0.

$$s_1 = \tilde{\gamma}_R\left(1-\frac{\tilde{V}_R}{V_g}\right)^2, \tag{19}$$

$$s_2 = \frac{1}{2\xi\chi}\left\{\tilde{\gamma}_R\tilde{\omega}\left(\frac{V_{\perp 0}}{c}\right)^2 - \left[2+\chi^2\frac{(1-\tilde{\gamma}_R\tilde{\omega})}{(1-\tilde{\omega})}\right]\frac{\tilde{V}_R V_P}{c^2}\right\}, \tag{20}$$

$$\tilde{a} = \frac{4.5}{(LR_E)^2}\left(\frac{c}{\Omega_e}\right)^2, \quad \frac{V_P}{c} = \chi\xi, \tag{21}$$

where V_P is the wave phase speed.

Equations (16) and (17) hold at the magnetic equator of an assumed dipole field, and in general for wave frequencies in the range $0.1 \le \tilde{\omega} \le 0.5$. The parameter $\tilde{a}$ in Eq. (21) arises from a Taylor expansion of the Earth's dipole magnetic field about the equator; L denotes magnetic shell and R_E is the Earth's radius. For self-sustaining emissions to exist, the wave amplitude must satisfy a threshold condition. By setting $\partial\tilde{B}_w/\partial\tilde{t} = 0$ in Eq. (16) and then solving for B_w, we determine that the normalized threshold wave amplitude ($\tilde{B}_{th} = B_{th}/B_0$) is given by

$$\tilde{B}_{th} = 50\pi^3\left(\frac{1-\beta^{3/2}}{1-\beta}\right)^2\left(\frac{N_0}{N_h}\right)^2\left(\frac{\tilde{a}s_2}{Q}\right)^2 \frac{\tilde{\gamma}_R^3\xi}{\tilde{\omega}\chi^5}\left(\frac{c}{V_{\perp 0}}\right)^5\left(\frac{\theta_\parallel}{m_e c}\right)^2 a^2\exp\left(\frac{2\tilde{p}_R^2}{\theta_\parallel^2}\right). \tag{22}$$

In Fig. 5, we present two-dimensional plots of the normalized threshold wave amplitude $\tilde{B}_{th}$ as a function of the cold-plasma parameter a and the thermal anisotropy A_T, for $N_h/N_0 = 10^{-2}$, 10^{-3}, and 10^{-4}. The white regions represent regions of parameter space corresponding to unreasonably large values of $\tilde{B}_{th}$. It is clear that $\tilde{B}_{th}$ can be strongly dependent on a, subject to the particular values of N_h/N_0 and A_T considered. When N_h/N_0 decreases, reasonable values of $\tilde{B}_{th}$ are obtained in the region typified by smaller a values and larger A_T values.

In general, Eqs. (16) and (17) are solved as an initial-value problem for $\tilde{B}_w(\tilde{t})$ and $\tilde{\omega}(\tilde{t})$, subject to the initial condition $\tilde{\omega}(0) = \tilde{\omega}_0$ and $\tilde{B}_w(0) = B_w(0)/B_0$, where $\tilde{\omega}_0$ is the initial wave frequency and $\tilde{B}_w(0)$ is chosen to be greater than the value of $\tilde{B}_{th}$ calculated from Eq. (22) corresponding to $\tilde{\omega}_0$.

The nonlinear growth rate Γ_N specified by Eqs. (5) and (6) can be regarded as a "total" growth rate since $\mathrm{d}/\mathrm{d}t \equiv \partial/\partial t + V_g\partial/\partial h$, where h is the distance measured along the magnetic field line from the magnetic equator. Following Summers et al. (2012a, 2013), we define a "temporal" nonlinear growth rate γ_N given by

$$\frac{\partial B_w}{\partial t} = \gamma_N B_w, \tag{23}$$

where

$$\gamma_N = \Gamma_N - 5\frac{|\Omega_e|}{\tilde{B}_w}\frac{s_2}{s_0}\frac{V_g}{c}\frac{\tilde{a}}{\tilde{\omega}}. \tag{24}$$

Since the temporal linear growth rate ω_i satisfies

$$\frac{\partial B_w}{\partial t} = \omega_i B_w, \tag{25}$$

then Eqs. (25) and (23) are analogous and respectively describe wave growth during the linear and nonlinear phases. We can construct complete time profiles for B_w by a suitable matching of the linear and nonlinear solutions at the interface of the linear and nonlinear regimes. We describe this procedure in the following section.

4 Linear–nonlinear matching region

In order to construct a complete time profile of B_w, we assume that linear wave growth smoothly merges into nonlinear wave growth at a particular wave amplitude $\tilde{B}_m = B_m/B_0$ which we call the matching wave amplitude. We assume that the smooth matching occurs when

$$\gamma_N = (\omega_i)_{max}\,, \tag{26}$$

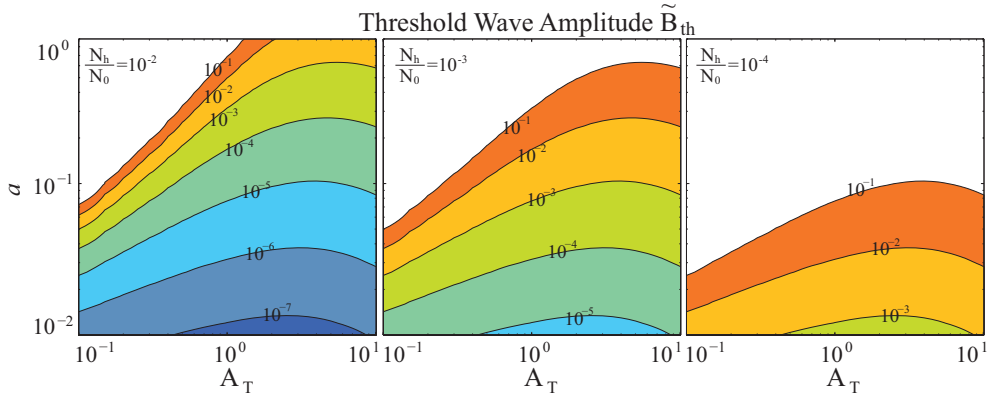

Figure 5. Two-dimensional plots of the threshold wave amplitude $\tilde{B}_{th} = B_{th}/B_0$, as a function of the cold-plasma parameter $a = |\Omega_e|^2/\omega_{pe}^2$ and thermal anisotropy A_T, for the indicated values of the electron number density ratio N_h/N_0.

where γ_N is the local nonlinear growth rate given by Eq. (24) and $(\omega_i)_{max}$ is the maximum value of the relativistic linear growth rate. It then follows from Eqs. (6), (24) and (26) that the matching wave amplitude is given by

$$A_1\sqrt{X} - B_1 - C_1 X = 0, \tag{27}$$

where $X = \tilde{B}_m$, and

$$A_1 = k_1\left(\frac{N_h}{N_0}\right),\ B_1 = k_2,\ C_1 = k_3\left(\frac{N_h}{N_0}\right). \tag{28}$$

The parameters k_1 and k_2 are evaluated at $\tilde{\omega} = \tilde{\omega}_m = \omega_m/|\Omega_e|$ where ω_m is the frequency at which the linear growth rate maximizes; $\tilde{\omega}_m$, k_1, k_2 and k_3 can each be regarded as a function of A_T, $\theta_\parallel/(m_e c)$, and the cold-plasma parameter a. The detailed algebraic expressions for k_1, k_2 and k_3 are given in Appendix A. From Eq. (27) we find

$$X = \tilde{B}_m = \left(\frac{A_1 \pm \sqrt{A_1^2 - 4B_1C_1}}{2C_1}\right)^2, \tag{29}$$

where we select the lower $(-)$ root sign.

From Eq. (29) we see that the matching process is only possible if $A_1^2 - 4B_1C_1 \geq 0$, which is equivalent to $N_h/N_0 \geq 4k_2k_3/k_1^2$. Construction of the "matching boundary", $N_h/N_0 = 4k_2k_3/k_1^2$, and hence the linear–nonlinear matching region in the $(N_h/N_0, A_T)$ plane is straightforward since the parameters k_1, k_2 and k_3 are functions of A_T only, for fixed values of a and $\theta_\parallel/(m_e c)$.

In Fig 6, top panels, we show the matching boundary $N_h/N_0 = 4k_2k_3/k_1^2$ (black curve) and the (blue) region over which linear–nonlinear matching is possible, for the specified values of a. Corresponding to each case in the top panel, we show in the bottom panel the dependence on the thermal anisotropy A_T of the wave frequency $\tilde{\omega}_m = \omega_m/|\Omega_e|$ at which the relativistic linear growth rate maximizes. When a increases (or N_0 decreases) the matching region is seen to shift toward the top-right region of $(N_h/N_0, A_T)$ space corresponding to larger N_h/N_0 values and larger A_T values. Thus for a lower cold electron number density, more energetic particles are needed to enable the linear–nonlinear matching process.

Motivated by a series of electron hybrid simulations of whistler-mode chorus by Katoh and Omura (2011), Summers et al. (2013) proposed that the boundary separating linear wave growth and nonlinear wave growth can be given by the relation

$$\max(\omega_i/|\Omega_e|) = M, \tag{30}$$

where M is a fixed bound. The criterion in Eq. (30) implies that linear wave growth only occurs when initial linear growth rates satisfy $\max(\omega_i/|\Omega_e|) < M$, while nonlinear wave growth occurs when linear growth rates satisfy $\max(\omega_i/|\Omega_e|) > M$.

Summers et al. (2013) showed that Eq. (30) can be written as

$$\frac{N_h}{N_0} = \frac{M}{c_1(A_T - c_2)}, \tag{31}$$

where the parameters c_1 and c_2 are relatively weak functions of the thermal anisotropy A_T. For given values of a and $\theta_\parallel/(m_e c)$, we can readily construct the boundary curve in Eq. (31) in the $(N_h/N_0, A_T)$ plane and hence determine the region $N_h/N_0 > M/[c_1(A_T - c_2)]$ in which nonlinear chorus occurs.

In Fig. 7, for the indicated values of a, we plot Eq. (31) with $M = 10^{-3}$ as a red curve, which acts as the boundary of the pink region representing $\max(\omega_i/|\Omega_e|) > 10^{-3}$ in which nonlinear wave growth takes place. In each panel we superimpose on top of the pink region the relevant blue (linear–nonlinear matching) region depicted in Fig. 6. Evidently the linear–nonlinear matching procedure does not in general apply throughout the nonlinear chorus growth region. As in Fig. 6, when a increases, the nonlinear chorus growth region

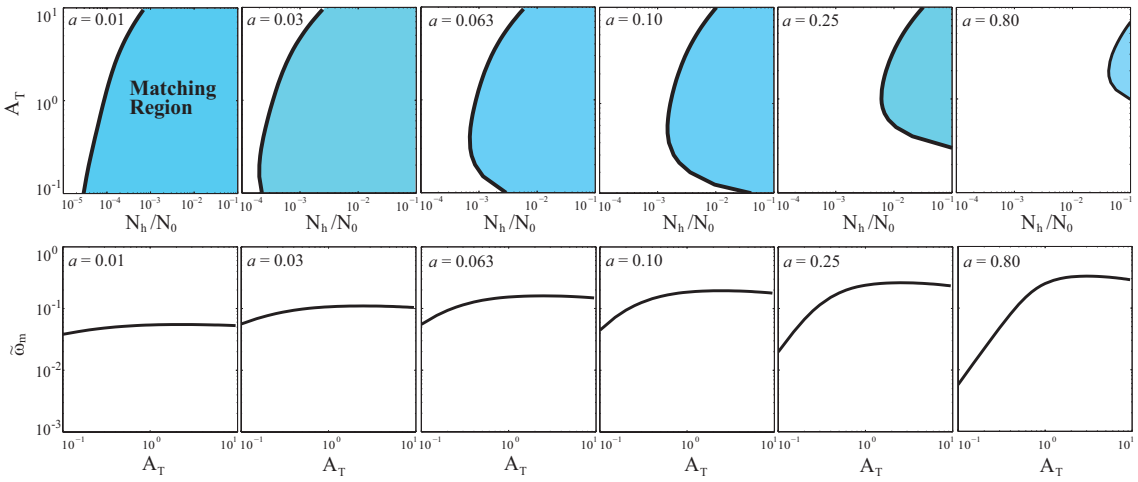

Figure 6. (a) Top panels show the matching boundary $N_h/N_0 = 4k_2k_3/k_1^2$ (black curve) and the (blue) region over which linear–nonlinear matching is possible, for the specified values of $a = |\Omega_e|^2/\omega_{pe}^2$. **(b)** Bottom panels show the dependence on the thermal anisotropy A_T of the wave frequency $\tilde{\omega}_m = \omega_m/|\Omega_e|$ at which the relativistic linear growth rate maximizes.

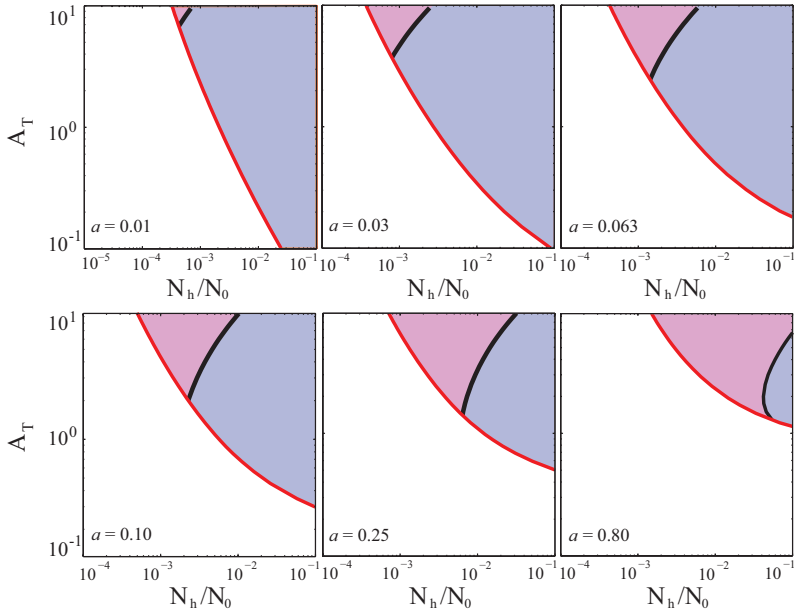

Figure 7. Variation of the parameter space for nonlinear whistler-mode wave growth with respect to the cold-plasma parameter $a = |\Omega_e|^2/\omega_{pe}^2$. The red boundary corresponds to Eq. (31) with $M = 10^{-3}$. In the pink region above the red boundary, nonlinear wave growth occurs, while in the white region only linear growth occurs. Superimposed on the pink region of nonlinear growth are the blue linear–nonlinear matching regions shown in Fig. 6.

in $(N_h/N_0, A_T)$ space shifts to the top-right region of larger N_h/N_0 values and larger A_T values.

In Fig. 8, we present four sets of three panels, for the respective parameter values $a = 0.04$, 0.06, 0.08, and 0.1, showing linear–nonlinear matching wave amplitude profiles. Also shown are corresponding profiles of the wave frequency $\omega(t)$ during the nonlinear phase and the local nonlinear wave growth rate $\gamma_N(t)$. Values of the electron number density ratio N_h/N_0 are selected in the range 7.5×10^{-4} to 2.5×10^{-3}. Construction of the matching profiles involves matching nonlinear solutions of the chorus Eqs. (16)–(17) to appropriate linear solutions of Eq. (25). In the solution of Eqs. (16)–(17), we apply the initial conditions $\tilde{\omega}(0) = \tilde{\omega}_0 = \tilde{\omega}_m$, $\tilde{B}_w(0) = \tilde{B}_m$, where $\tilde{\omega}_m$ is the wave frequency at which the linear growth rate maximizes and $\tilde{B}_m$ is the matching wave amplitude given by Eq. (29). We see from Fig. 8 that as the parameter a increases, the matching wave amplitude increases and the linear–nonlinear matching process is only possible for

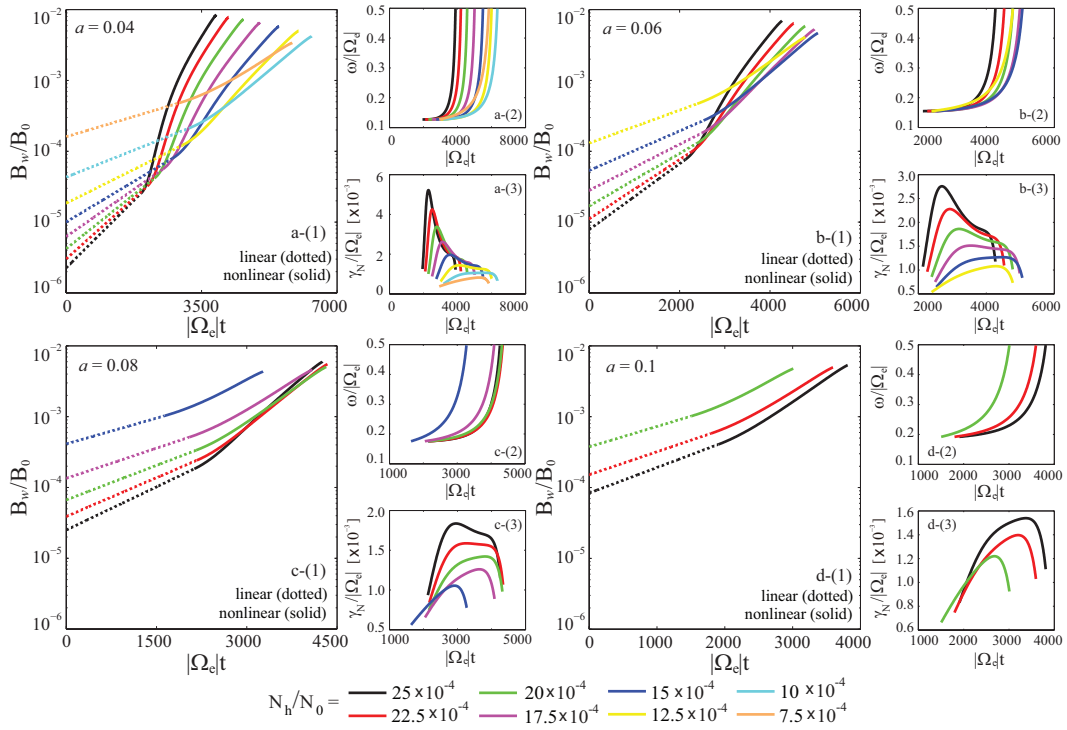

Figure 8. Panels **a-(1)**, **b-(1)**, **c-(1)**, and **d-(1)** show the time variation of the whistler-mode wave magnetic field B_w comprising smoothly matched linear and nonlinear profiles, for the specified values of the cold-plasma parameter $a = |\Omega_e|^2/\omega_{pe}^2$ and the electron number density ratio N_h/N_0. Panels **a-(2)**, **b-(2)**, **c-(2)**, and **d-(2)** show the corresponding time profiles of the wave frequency ω, and panels **a-(3)**, **b-(3)**, **c-(3)**, and **d-(3)** show the local nonlinear growth rate γ_N.

sufficiently large values of N_h/N_0. As well, as a increases, the maximum values of the nonlinear growth rate γ_N decline, and the profiles of γ_N become flatter. The results in Fig. 8 reinforce the conclusion from Fig. 7 that the conditions for nonlinear wave growth generally become less favorable as the parameter a increases.

5 Conclusions

We have considered the linear and nonlinear growth of magnetospheric whistler-mode waves as the parameter $a = |\Omega_e|^2/\omega_{pe}^2$ varies. Since $a \propto B_0^2/N_0$, where N_0 is the cold electron number density and B_0 is the background magnetic field strength, then at a given L shell or fixed magnetic field, an increasing (decreasing) value of a implies a decreasing (increasing) value of the cold electron number density. Our general conclusions are as follows:

1. As the parameter a increases, the maximum linear growth rate decreases, for given values of the thermal anisotropy A_T and the ratio N_h/N_0, where N_h is the hot (energetic) electron number density.

2. As a increases, the threshold wave amplitude $\tilde{B}_{th}$ (given by Eq. 22) for nonlinear wave growth increases, for given values of A_T and N_h/N_0.

3. As a increases, the matching wave amplitude $\tilde{B}_m$ (given by Eq. 29) occurring at the transition from linear to nonlinear growth increases, for given values of A_T and N_h/N_0.

4. As a increases, the maximum value of the nonlinear growth rate γ_N (given by Eq. 24) decreases, for given values of A_T and N_h/N_0.

5. The region of $(N_h/N_0, A_T)$ space that is favorable to nonlinear whistler-mode wave growth becomes more restricted as the parameter a increases. Specifically, as a increases, the region permitting nonlinear wave growth shifts toward the top right of $(N_h/N_0, A_T)$ space characterized by larger N_h/N_0 values and larger A_T values.

6. This study sharpens the realization that the nonlinear growth of whistler-mode waves is only possible over a relatively restricted region of the three-dimensional $(N_h/N_0, A_T, a)$-parameter space. The results reported here serve as an aid in choosing input parameters for computationally intensive particle simulations, and also as a practical tool to assist in the analysis of experimental whistler-mode wave data.

Appendix A: Detailed form of the parameters k_1, k_2, and k_3 appearing in Eqs. (27) and (28)

The parameters k_1, k_2, k_3 are given by

$$k_1 = \sqrt{2}\left(\frac{1-\beta}{1-\beta^{3/2}}\right) Q\chi^{3/2}\left(\frac{\xi}{\tilde{\gamma}_R}\right)^{1/2} \frac{1}{\tilde{\omega}^{1/2}}\left(\frac{V_g}{c}\right) \left(\frac{V_{\perp 0}}{c}\right)^{5/2} \frac{1}{\pi^2 a}\left(\frac{m_e c}{\theta_\parallel}\right)\left(\frac{m_e c}{\theta_\perp}\right) \exp\left(-\frac{\tilde{p}_R^2}{\theta_\parallel^2}\right), \quad \text{(A1)}$$

$$k_2 = 5\frac{s_2}{s_0}\left(\frac{V_g}{c}\right)\left(\frac{\tilde{a}}{\tilde{\omega}}\right), \quad \text{(A2)}$$

$$k_3 = 2\sqrt{\pi}\left(\frac{m_e c}{\theta_\parallel}\right) \max\left\{\frac{(1-x)^2}{[1+2ax(1-x)^2]}[I_2 - \frac{x}{y}I_1]\right\}, \quad \text{(A3)}$$

where I_1 and I_2 are the integrals defined by

$$I_1(x,y) = \frac{1}{1-\beta}\int_0^\infty \frac{z^3 dz}{\Delta_R}\left[e^{-z^2} - \frac{1}{\beta}e^{-z^2/\beta}\right] \exp\left[-\left(\frac{1-\gamma_R x}{y}\right)^2\left(\frac{m_e c}{\theta_\parallel}\right)^2\right], \quad \text{(A4)}$$

and

$$I_2(x,y) = \frac{1}{1-\beta}\int_0^\infty \frac{z^3 dz}{\Delta_R \gamma_R}\left\{\left(\frac{A_T-\beta}{1+\beta}\right)e^{-z^2} - \left(\frac{\beta A_T - 1}{\beta(1+\beta)}\right)e^{-z^2/\beta}\right\}\left(\frac{1-\gamma_R x}{y}\right) \exp\left[-\left(\frac{1-\gamma_R x}{y}\right)^2\left(\frac{m_e c}{\theta_\parallel}\right)^2\right], \quad \text{(A5)}$$

$$\gamma_R = \frac{-x + y\left[(y^2-x^2)\left\{1+z^2\left(\frac{A_T+1}{1+\beta}\right)\left(\frac{\theta_\parallel}{m_e c}\right)^2\right\}+1\right]^{1/2}}{y^2-x^2} \quad \text{(A6)}$$

is the resonant value of the Lorentz factor, and

$$\Delta_R = 1 - \frac{x(\gamma_R x - 1)}{\gamma_R y^2} \quad \text{(A7)}$$

is the resonant denominator.

Acknowledgements. This work was supported by the National Science Foundation of China (NSFC) under grants 41331070, 41174147, the Specialized Research Fund for State Key Laboratories under grant 201309FSK, the Specialized Research Fund for the Doctoral Program of Higher Education under grant 20133601120005, and the Educational Foundation of Jiangxi Province under grant GJJ13050. D. Summers was supported by a Discovery Grant of the Natural Sciences and Engineering Research Council of Canada. We thank Y. Omura for useful discussions.

Topical Editor E. Roussos thanks one anonymous referee for his/her help in evaluating this paper.

References

Ashour-Abdalla, M. and Kennel, C. F.: Nonconvective and convective electron cyclotron harmonic instabilities, J. Geophys. Res., 83, 1531, doi:10.1029/JA083iA04p01531, 1978.

Dory, R. A., Guest, G. E., and Harris, E. G.: Unstable electrostatic plasma waves propagating perpendicular to a magnetic field, Phys. Rev. Lett., 14, 131, doi:10.1103/PhysRevLett.14.131, 1965.

Hikishima, M., Yagitani, S., Omura, Y., and Nagano I.: Full particle simulation of whistler-mode rising chorus emissions in the magnetosphere, J. Geophys. Res., 114, A01203, doi:10.1029/2008JA013625, 2009.

Hikishima, M., Omura, Y., and Summers, D.: Microburst precipitation of energetic electrons associated with chorus wave generation, Geophys. Res. Lett., 37, L07103, doi:10.1029/2010GL042678, 2010.

Katoh, Y. and Omura Y.: Amplitude dependence of frequency sweep rates of whistler mode chorus emissions, J. Geophys. Res., 116, A07201, doi:10.1029/2011JA016496, 2011.

Kennel, C. F. and Petschek, H. E.: Limit on stably trapped particle fluxes, J. Geophys. Res., 71, 1–28, doi:10.1029/JZ071i001p00001, 1966.

Lorentzen, K. R., Blake, J. B., Inan, U. S., and Bortnik, J.: Observations of relativistic electron microbursts in association with VLF chorus, J. Geophys. Res., 106, 6017, doi:10.1029/2000JA003018, 2001.

Mauk, B. H. and Fox, N. J.: Electron radiation belts of the solar system, J. Geophys. Res., 115, A12220, doi:10.1029/2010JA015660, 2010.

Meredith, N. P., Cain, M., Horne, R. B., Thorne, R. M., Summers, D., and Anderson, R. R.: Evidence for chorus-driven electron acceleration to relativistic energies from a survey of geomagnetically disturbed periods, J. Geophys. Res., 108, 1248, doi:10.1029/2002JA009764, 2003.

Ni, B., Thorne, R. M., Shprits, Y. Y., and Bortnik, J.: Resonant scattering of plasma sheet electrons by whistler-mode chorus: Contribution to diffuse auroral precipitation, Geophys. Res. Lett., 35, L11106, doi:10.1029/2008GL034032, 2008.

O'Brien, T. P., Looper, M. D., and Blake, J. B.: Quantification of relativistic electron microburst losses during the GEM storms, Geophys. Res. Lett., 31, L04802, doi:10.1029/2003GL018621, 2004.

Omura, Y., Katoh, Y., and Summers, D.: Theory and simulation of the generation of whistler-mode chorus, J. Geophys. Res., 113, A04223, doi:10.1029/2007JA012622, 2008.

Omura, Y., Hikishima, M., Katoh, Y., Summers, D., and Yagitani, S.: Nonlinear mechanisms of lower-band and upper-band VLF chorus emissions in the magnetosphere, J. Geophys. Res., 114, A07217, doi:10.1029/2009JA014206, 2009.

Omura, Y., Nunn, D., and Summers, D.: Generation processes of whistler mode chorus emissions: Current status of nonlinear wave growth theory, in: Dynamics of the Earth's Radiation Belts and Inner Magnetosphere, Geophys. Monogr. Ser., 199, edited by: Summers D., Mann I. R., Baker D. N., and Schulz M., AGU, Washington, DC, 243–254, doi:10.1029/2012GM001347, 2012.

Roth, I., Temerin, M., and Hudson, M. K.: Resonant enhancement of relativistic electron fluxes during geomagnetically active periods, Ann. Geophys., 17, 631–638, doi:10.1007/s00585-999-0631-2, 1999.

Su, Z., Xiao, F., Zheng, H., He, Z., Zhu, H., Zhang, M., Shen, C., Wang, Y., Wang, S., Kletzing, C. A., Kurth, W. S., Hospodarsky, G. B., Spence, H. E., Reeves, G. D., Funsten, H. O., Blake, J. B., and Baker, D. N.: Nonstorm time dynamics of electron radiation belts observed by the Van Allen Probes, Geophys. Res. Lett., 41, 229, doi:10.1002/2013GL058912, 2014.

Summers, D. and Omura, Y.: Ultra-relativistic acceleration of electrons in planetary magnetospheres, Geophys. Res. Lett., 34, L24205, doi:10.1029/2007GL032226, 2007.

Summers, D., Thorne, R. M., and Xiao, F.: Relativistic theory of wave-particle resonant diffusion with application to electron acceleration in the magnetosphere, J. Geophys. Res., 103, 20487, doi:10.1029/98JA01740, 1998.

Summers, D., Ma, C., Meredith, N. P., Horne, R. B., Thorne, R. M., Heynderickx, D., and Anderson, R. R.: Model of the energization of outer-zone electrons by whistler-mode chorus during the October 9, 1990 geomagnetic storm, Geophys. Res. Lett., 29, 2174, doi:10.1029/2002GL016039, 2002.

Summers, D., Ni, B., and Meredith, N. P.: Timescales for radiation belt electron acceleration and loss due to resonant wave-particle interactions: 1. Theory, J. Geophys. Res., 112, A04206, doi:10.1029/2006JA011801, 2007a.

Summers, D., Ni, B., and Meredith, N. P.: Timescales for radiation belt electron acceleration and loss due to resonant wave-particle interactions: 2. Evaluation for VLF chorus, ELF hiss, and electromagnetic ion cyclotron waves, J. Geophys. Res., 112, A04207, doi:10.1029/2006JA011993, 2007b.

Summers, D., Tang, R., and Thorne, R. M.: Limit on stably trapped particle fluxes in planetary magnetospheres, J. Geophys. Res., 114, A10210, doi:10.1029/2009JA014428, 2009.

Summers, D., Tang, R., and Omura, Y.: Effects of nonlinear wave growth on extreme radiation belt electron fluxes, J. Geophys. Res., 116, A10226, doi:10.1029/2011JA016602, 2011.

Summers, D., Tang, R., and Omura, Y.: Linear and nonlinear growth of magnetospheric whistler mode waves, in: Dynamics of the Earth's Radiation Belts and Inner Magnetosphere, Geophys. Monogr. Ser., 199, edited by: Summers D., Mann I. R., Baker D. N., and Schulz M., AGU, Washington, DC, 265–279, doi:10.1029/2012GM001298, 2012a.

Summers, D., Omura, Y., Miyashita, Y., and Lee, D.-H.: Nonlinear spatiotemporal evolution of whistler mode chorus waves in Earth's inner magnetosphere, J. Geophys. Res., 117, A09206, doi:10.1029/2012JA017842, 2012b.

Summers, D., Tang, R., Omura, Y., and Lee, D.-H.: Parameter spaces for linear and nonlinear whistler-mode waves, Phys. Plasmas, 20, 072110, doi:10.1063/1.4816022, 2013.

Tang, R. and Summers, D.: Energetic electron fluxes at Saturn from Cassini observations, J. Geophys. Res., 117, A06211, doi:10.1029/2011JA017394, 2012.

Thorne, R. M., O'Brien, T. P., Shprits, Y. Y., Summers, D., and Horne, R. B.: Timescale for MeV electron microburst loss during geomagnetic storms, J. Geophys. Res., 110, A09202, doi:10.1029/2004JA010882, 2005.

Xiao, F., Su, Z., Zheng, H., and Wang, S.: Three-dimensional simulations of outer radiation belt electron dynamics including cross-diffusion terms, J. Geophys. Res., 115, A05216, doi:10.1029/2009JA014541, 2010.